Lax pair and vector semi-rational nonautonomous rogue waves for a coupled time-dependent coefficient fourth-order nonlinear Schrödinger system in an inhomogeneous optical fiber*

Zhong Du(杜仲)[1], Bo Tian(田播)[1,†], Qi-Xing Qu(屈启兴)[2], and Xue-Hui Zhao(赵学慧)[1]

[1] State Key Laboratory of Information Photonics and Optical Communications, and School of Science, Beijing University of Posts and Telecommunications, Beijing 100876, China

[2] School of Information, University of International Business and Economics, Beijing 100029, China

(Received 18 December 2019; revised manuscript received 7 January 2020; accepted manuscript online 10 February 2020)

Optical fibers are seen in the optical sensing and optical fiber communication. Simultaneous propagation of optical pulses in an inhomogeneous optical fiber is described by a coupled time-dependent coefficient fourth-order nonlinear Schrödinger system, which is discussed in this paper. For such a system, we work out the Lax pair, Darboux transformation, and corresponding vector semi-rational nonautonomous rogue wave solutions. When the group velocity dispersion (GVD) and fourth-order dispersion (FOD) coefficients are the constants, we exhibit the first- and second-order vector semi-rational rogue waves which are composed of the four-petalled rogue waves and eye-shaped breathers. Both the width of the rogue wave along the time axis and temporal separation between the adjacent peaks of the breather decrease with the GVD coefficient or FOD coefficient. With the GVD and FOD coefficients as the linear, cosine, and exponential functions, we respectively present the first- and second-order periodic vector semi-rational rogue waves, first- and second-order asymmetry vector semi-rational rogue waves, and interactions between the eye-shaped breathers and the composite rogue waves.

Keywords: inhomogeneous optical fiber, Lax pair, coupled time-dependent coefficient fourth-order nonlinear Schrödinger system, vector semi-rational nonautonomous rogue waves, breathers

PACS: 02.30.Ik, 42.65.Tg, 04.30.Nk **DOI:** 10.1088/1674-1056/ab7442

1. Introduction

Optical fibers have been seen in the optical sensing and optical fiber communication.[1] Optical solitons, caused by the balance between self-phase modulation (SPM) and group velocity dispersion (GVD) effects, have been applied in the fields of optical fiber communication, nonlinear optics, optical information processing, and photonic computing.[2–7] Under certain conditions, breathers, which can periodically propagate in the nonlinear media, have been shown to convert into solitons.[8–11] Rogue waves have been thought as a kind of special soliton solutions, which can store certain energy and enlarge the optical pulses.[12–16]

Optical pulse propagation inside a one-mode optical fiber has been found to be described by the scalar nonlinear Schrödinger (NLS)-type equation containing the SPM and GVD effects.[17] Scalar NLS-type equation has been verified to model the solitons, breathers, and rogue waves.[18–20] For modeling the semi-rational vector rogue waves which can describe that breathers or solitons coexist with the rogue waves, the scalar NLS-type equation has been extended to the coupled NLS-type system.[22–24] Besides, more types of vector rational rogue waves such as the anti-eye-shaped rogue waves and four-petaled rogue waves have been found to be modeled by the coupled systems.[22–27]

The NLS-type equations with the variable coefficients have been called to describe the nonlinear waves including the solitons, breathers, and rogue waves.[28] For the simultaneous propagation of optical pulses in an inhomogeneous optical fiber, references [29–31] have discussed the coupled time-dependent coefficient fourth-order NLS system

$$\begin{aligned}&\mathrm{i}q_{1,t}+\mu(t)q_{1,xx}+\nu(t)q_1\sum_{\rho=1}^{2}|q_\rho|^2+\gamma(t)q_{1,xxxx}\\&+\gamma_1(t)q_1\sum_{\rho=1}^{2}|q_{\rho,x}|^2+\gamma_2(t)q_{1,x}\sum_{\rho=1}^{2}q_\rho q_{\rho,x}^*\\&+\gamma_3(t)q_{1,x}\sum_{\rho=1}^{2}q_\rho^* q_{\rho,x}+\gamma_4(t)q_{1,xx}\sum_{\rho=1}^{2}|q_\rho|^2\\&+\gamma_5(t)q_1\sum_{\rho=1}^{2}q_\rho^* q_{\rho,xx}+\gamma_6(t)q_1\sum_{\rho=1}^{2}q_\rho q_{\rho,xx}^*\\&+\gamma_7(t)q_1\left(\sum_{\rho=1}^{2}|q_\rho|^2\right)^2=0,\end{aligned}\tag{1a}$$

$$\mathrm{i}q_{2,t}+\mu(t)q_{2,xx}+\nu(t)q_2\sum_{\rho=1}^{2}|q_\rho|^2$$

*Project supported by the BUPT Excellent Ph.D. Students Foundation (Grant No. CX2019201), the National Natural Science Foundation of China (Grant Nos. 11772017 and 11805020), the Fund of State Key Laboratory of Information Photonics and Optical Communications (Beijing University of Posts and Telecommunications), China (Grant No. IPOC: 2017ZZ05), and the Fundamental Research Funds for the Central Universities of China (Grant No. 2011BUPTYB02).

†Corresponding author. E-mail: tian_bupt@163.com

$$+\gamma(t)\,q_{2,xxxx}+\gamma_1(t)\,q_2\sum_{\rho=1}^{2}|q_{\rho,x}|^2+\gamma_2(t)\,q_{2,x}\sum_{\rho=1}^{2}q_\rho q^*_{\rho,x}$$
$$+\gamma_3(t)\,q_{2,x}\sum_{\rho=1}^{2}q^*_\rho q_{\rho,x}+\gamma_4(t)\,q_{2,xx}\sum_{\rho=1}^{2}|q_\rho|^2$$
$$+\gamma_5(t)\,q_2\sum_{\rho=1}^{2}q^*_\rho q_{\rho,xx}+\gamma_6(t)\,q_2\sum_{\rho=1}^{2}q_\rho q^*_{\rho,xx}$$
$$+\gamma_7(t)\,q_2\Big(\sum_{\rho=1}^{2}|q_\rho|^2\Big)^2=0, \tag{1b}$$

where $q_1(x,t)$ and $q_2(x,t)$ are the complex envelopes of two field polarization components, "$*$" implies the complex conjugate, the subscripts stand for the partial derivatives to the normalized propagation distance x and retarded time t, respectively, $\mu(t)$ denotes the GVD coefficient, $\nu(t)$ represents the SPM coefficient, $\gamma(t)$ denotes the fourth-order dispersion (FOD) coefficient, $\gamma_s(t)$'s are the cubic nonlinear coefficients ($s=1,2,\ldots,6$), and $\gamma_7(t)$ represents the quintic nonlinear coefficient. For system (1), reference [29] has presented the cubic, periodic, parabolic and bound-state solitons; reference [30] has given the Lax pair and non-degenerate dark-dark solitons; reference [31] has reported the first- and second-order eye-shaped rogue waves.

However, the vector semi-rational nonautonomous rogue wave solutions for system (1), which can describe the existence of the four-petalled rogue waves and breathers, have not been constructed. In Section 2, with symbolic computation,[32–36] we will give out a Lax pair for system (1) which is distinct from that in Ref. [30], and the corresponding Darboux transformation (DT). In Section 3, we will derive the vector semi-rational nonautonomous rogue wave solutions for system (1). In Section 4, we will investigate the first- and second-order vector semi-rational nonautonomous rogue waves with the GVD and FOD coefficients. Our conclusions will be summarized in Section 5.

2. Lax pair and the N-th-order DT

Via the Ablowitz–Kaup–Newell–Segur method,[37] we work out another Lax pair for system (1) which is distinct from that in Ref. [30] as

$$\Psi_x=U\Psi,\quad \Psi_t=V\Psi, \tag{2}$$

where Ψ is the 3×1 vector complex eigenfunction of x, t and the complex eigenvalue λ,

$$\begin{aligned}U&=\mathrm{i}\left[\lambda(\Omega+I)+Q\right],\\ V&=-8\mathrm{i}\gamma(t)(\Omega+I)\lambda^4-8\mathrm{i}\gamma(t)Q\lambda^3\\ &\quad+2\left[2\mathrm{i}\gamma(t)Q^2\Omega-2\gamma(t)\Omega Q_x+\mathrm{i}\mu(t)(\Omega+I)\right]\lambda^2\\ &\quad+2\left[\mathrm{i}\gamma(t)Q_{xx}+2\mathrm{i}\gamma(t)Q^3-\gamma(t)QQ_x+\gamma(t)Q_xQ+\mathrm{i}\mu(t)Q\right]\lambda\\ &\quad+\gamma(t)\Omega Q_{xxx}-\mathrm{i}\gamma(t)\Omega QQ_{xx}-\mathrm{i}\gamma(t)\Omega Q_{xx}Q-3\mathrm{i}\gamma(t)\Omega Q^4\\ &\quad-\mathrm{i}\mu(t)\Omega Q^2+\mathrm{i}\gamma(t)Q_x^2\Omega+3\gamma(t)Q^2Q_x\\ &\quad+3\gamma(t)\Omega Q_xQ^2+\mu(t)\Omega Q_x+\mathrm{i}cI,\end{aligned}$$
$$Q=\begin{pmatrix}0&\frac{\beta}{2}q_1^*&\frac{\beta}{2}q_2^*\\ q_1&0&0\\ q_2&0&0\end{pmatrix},\quad \Omega=\begin{pmatrix}1&0&0\\0&-1&0\\0&0&-1\end{pmatrix},$$

I is the identity matrix, and c and β are both the constants. With the following coefficient conditions:[29]

$$\begin{aligned}&\nu(t)=\beta\mu(t),\ \ \gamma_1(t)=\beta\gamma(t),\ \ \gamma_2(t)=\beta\gamma(t),\\ &\gamma_3(t)=3\beta\gamma(t),\ \ \gamma_4(t)=2\beta\gamma(t),\ \ \gamma_5(t)=2\beta\gamma(t),\\ &\gamma_6(t)=\beta\gamma(t),\ \ \gamma_7(t)=\frac{3}{2}\beta^2\gamma(t),\end{aligned} \tag{3}$$

the zero curvature equation $U_t-V_x+UV-VU=0$ can yield system (1).

Based on the loop method and DT construction developed in Refs. [25–27], we construct the N-th-order DT matrix for system (1) as

$$D[N]=I-\Theta\mathscr{M}^{-1}(\lambda I-S)^{-1}\Theta^\dagger J,$$

and work out the N-th-order DT for system (1) as

$$Q[N]=Q+\Omega\Theta\mathscr{M}^{-1}\Theta^\dagger J-\Theta\mathscr{M}^{-1}\Theta^\dagger J\Omega, \tag{4}$$

where N is a positive integer, $[N]$ denotes the N-th iteration, $D[N]$ and $Q[N]$ are the 3×3 matrices, $\Theta=(y_1,y_2,\ldots,y_N)$, $\mathscr{M}=(M_{jk})_{N\times N}$ $(j,k=1,2,\ldots,N)$, $J=\mathrm{diag}(1,\beta/2,\beta/2)$, $M_{jk}=y_j^\dagger Jy_k/(\lambda_k-\lambda_j^*)$, $y_k\equiv y(x,t,\lambda_k)$, $y(x,t,\lambda)=v(x,t,\lambda)\Psi(x,t,\lambda)$, $v(x,t,\lambda)$ is a nonzero complex function, $\Psi(x,t,\lambda_k)$ is a 3×1 vector solution of Lax pair (2) at $\lambda=\lambda_k$, λ_k's are N given values of λ, $S=\mathrm{diag}(\lambda_1^*,\lambda_2^*,\ldots,\lambda_N^*)$, the superscript -1 stands for the inverse of a matrix, and the superscript $\dagger$ denotes the Hermitian conjugation.

In order to construct the expressions of $y(x,t,\lambda)$, we begin our analysis with the seed solutions for system (1) in the form

$$q_\alpha=a_\alpha\,\mathrm{e}^{\mathrm{i}[b_\alpha x+c_\alpha(t)]},\quad(\alpha=1,2), \tag{5}$$

where a_α's and b_α's are the real constants,

$$\begin{aligned}c_\alpha(t)&=\int\left[\beta(a_1^2+a_2^2)-b_\alpha^2\right]\mu(t)\,\mathrm{d}t\\ &\quad+\int\Big[b_\alpha^4-2\beta(a_1^2b_1+a_2^2b_2)b_\alpha-2\beta(a_1^2+a_2^2)b_\alpha^2\\ &\quad-2\beta(a_1^2b_1^2+a_2^2b_2^2)+\frac{3}{2}\beta^2(a_1^2+a_2^2)^2\Big]\gamma(t)\,\mathrm{d}t.\end{aligned}$$

Substituting seed solutions (5) into Lax pair (2), we find that the solutions of Lax pair (2) can be obtained as

$$\Psi(x,t,\lambda)=\mathscr{G}\mathscr{H}\mathscr{D}\mathscr{K}\mathscr{L}\,\mathrm{e}^{-\mathrm{i}\xi t}, \tag{6}$$

with

$$\mathscr{L}=(l_1,l_2,l_3)^{\mathrm{T}},$$

$$\mathscr{G}=\begin{pmatrix}1 & 0 & 0\\ 0 & a_1\,\mathrm{e}^{\mathrm{i}[b_1x+c_1(t)]} & 0\\ 0 & 0 & a_2\,\mathrm{e}^{\mathrm{i}[b_2x+c_2(t)]}\end{pmatrix},$$

$$\mathscr{H}=\begin{pmatrix}1 & 1 & 1\\ \frac{1}{b_1-z_1} & \frac{1}{b_1-z_2} & \frac{1}{b_1-z_3}\\ \frac{1}{b_2-z_1} & \frac{1}{b_2-z_2} & \frac{1}{b_2-z_3}\end{pmatrix},$$

$$\mathscr{K}=\begin{pmatrix}\mathrm{e}^{-\mathrm{i}f(z_1)} & 0 & 0\\ 0 & \mathrm{e}^{-\mathrm{i}f(z_2)} & 0\\ 0 & 0 & \mathrm{e}^{-\mathrm{i}f(z_3)}\end{pmatrix},$$

$$\mathscr{D}=\mathrm{diag}(\Pi_{\rho=1}^{2}(z_1-b_\rho),\ \Pi_{\rho=1}^{2}(z_2-b_\rho),\ \Pi_{\rho=1}^{2}(z_3-b_\rho)),$$

$$\xi=\left[\frac{3}{2}\beta^2c^2-2\beta\left(a_1^2b_1^2+a_2^2b_2^2\right)\right]\gamma(t)+[\beta\mu(t)-1]\,c,$$

$$f(\zeta)=\zeta x+\zeta^4\int\gamma(t)\,\mathrm{d}t-\zeta^2\int[2\beta c\gamma(t)+\mu(t)]\,\mathrm{d}t$$
$$-2\beta\zeta\int\left[a_1^2b_1\gamma(t)+a_2^2b_2\gamma(t)\right]\mathrm{d}t,$$

where $c=a_1^2+a_2^2$, l_1, l_2, and l_3 are all the nonzero constants, the superscript T means the transpose for a vector/matrix, and z_1, z_2, and z_3 are the three roots of the following cubic equation with respect to z:

$$z^3-\frac{1}{2}\left(a_1^2\beta+a_2^2\beta-2b_1b_2+4b_1\lambda+4b_2\lambda\right)z$$
$$-(b_1+b_2-2\lambda)z^2+\frac{1}{2}\left(a_1^2\beta b_2+a_2^2\beta b_1+4b_1b_2\lambda\right)=0. \quad (7)$$

We set $v(x,t,\lambda)=\mathrm{e}^{\mathrm{i}\xi t}$ and derive that

$$y(x,t,\lambda)=\mathscr{G}\mathscr{H}\mathscr{D}\mathscr{K}\mathscr{L}.$$

3. Vector semi-rational nonautonomous rogue wave solutions

Using the N-th-order DT (4) and the expansion method in Ref. [38], we will investigate the vector semi-rational nonautonomous rogue wave solutions for system (1) when cubic equation (7) admits two equal roots.

We take $\beta=2$, $a_1=a_2=1$, $b_1=2/5$, $b_2=-2/5$, and $\lambda=3\sqrt{6}\mathrm{i}/5$ such that we can derive two equal roots of cubic Eq. (7), i.e., $z_1=z_2=-\sqrt{6}\mathrm{i}/5$ and the other root, $z_3=-4\sqrt{6}\mathrm{i}/5$. According to the expansion method in Ref. [38], we assume that $\lambda=\lambda_1(1+\varepsilon^2)$ with ε being a small parameter. We set $\lambda_1=3\sqrt{6}\mathrm{i}/5$ and substitute $\beta=2$, $a_1=a_2=1$, $b_1=2/5$, $b_2=-2/5$, and $\lambda=\lambda_1(1+\varepsilon^2)$ into cubic Eq. (7) such that we work out three different roots of cubic Eq. (7),

$$z_1=\frac{1}{5}\sqrt{6}\left[\frac{(\mathrm{i}+\sqrt{3})\left(4\varepsilon^4+8\varepsilon^2+1\right)}{2\tau}+\frac{\mathrm{i}-\sqrt{3}}{2}\tau-2\mathrm{i}\left(\varepsilon^2+1\right)\right],$$

$$z_2=\frac{1}{5}\sqrt{6}\left[\frac{(\mathrm{i}-\sqrt{3})\left(4\varepsilon^4+8\varepsilon^2+1\right)}{2\tau}+\frac{\mathrm{i}+\sqrt{3}}{2}\tau-2\mathrm{i}\left(\varepsilon^2+1\right)\right],$$

$$z_3=-\frac{\mathrm{i}\sqrt{6}\left[2(\tau+4)\varepsilon^2+(\tau+1)^2+4\varepsilon^4\right]}{5\tau},$$

with

$$\tau=\sqrt[3]{8\varepsilon^6+24\varepsilon^4+17\varepsilon^2-\varepsilon\sqrt{32\varepsilon^6+128\varepsilon^4+133\varepsilon^2+10}+1}.$$

In what follows, we take

$$\mathscr{W}=\begin{pmatrix}1 & 1 & 0\\ 1 & -1 & 0\\ 0 & 0 & 1\end{pmatrix},\qquad \mathscr{R}=\begin{pmatrix}1 & 0 & 0\\ 0 & \frac{1}{\varepsilon} & 0\\ 0 & 0 & 1\end{pmatrix},$$

and $l_d=\sum_{j=1}^{N}l_{dj}\varepsilon^{2(j-1)}$ $(d=1,2,3)$ such that we can give out the following Taylor expansion of $\mathscr{H}\mathscr{D}\mathscr{K}\mathscr{W}\mathscr{R}\mathscr{L}$:

$$\mathscr{H}\mathscr{D}\mathscr{K}\mathscr{W}\mathscr{R}\mathscr{L}=\sum_{h=0}^{\infty}g_h(x,t)\varepsilon^{2j}, \quad (8)$$

with $g_h=\frac{1}{h!}\frac{\partial^h(\mathscr{H}\mathscr{D}\mathscr{K}\mathscr{W}\mathscr{R}\mathscr{L})}{\partial\lambda^h}\Big|_{\lambda=\frac{3\sqrt{6}\mathrm{i}}{5}}$ $(h=0,1,2,\ldots)$. According to the expansion method in Refs. [25–27,38], via the N-th-order DT (4) and expansion (8), we acquire the N-th-order vector semi-rational nonautonomous rogue wave solutions for system (1) as

$$q_1[N]=\mathrm{e}^{\mathrm{i}\left[\frac{2}{5}x+c_1(t)\right]}\frac{\det(\Gamma-2\Xi_1^{\dagger}\Xi_2)}{\det(\Gamma)}, \quad (9a)$$

$$q_2[N]=\mathrm{e}^{\mathrm{i}\left[-\frac{2}{5}x+c_2(t)\right]}\frac{\det(\Gamma-2\Xi_1^{\dagger}\Xi_3)}{\det(\Gamma)}, \quad (9b)$$

where $\Xi(x,t)=(g_0,g_1,\ldots,g_{N-1})$, Ξ_d denotes the d-th row of $\Xi(x,t)$, and $\Gamma=(\Gamma_{jk})_{N\times N}$ with

$$\Gamma_{jk}=\sum_{s=0}^{j+k-2}\sum_{n=\max(0,s-j+1)}^{\min(k-1,s)}\left(-\frac{5\sqrt{6}}{36}\mathrm{i}\right)^{s+1}\times C_s^n\left(-\frac{3\sqrt{6}\mathrm{i}}{5}\right)^{s}g_{j-1-s+n}^{\dagger}g_{k-1-n}.$$

4. Discussions on the vector semi-rational nonautonomous rogue waves

Under coefficient conditions (3), the N-th-order vector semi-rational nonautonomous rogue wave solutions for system (1), i.e., solutions (9), are only associated with the GVD coefficient $\mu(t)$ and FOD coefficient $\gamma(t)$. In what follows, we will study the properties of the first- and the second-order vector semi-rational nonautonomous rogue waves based on solutions (9) with $\mu(t)$ and $\gamma(t)$ chosen as the distinct functions.

4.1. The first-order vector semi-rational nonautonomous rogue waves

Figure 1 illustrates the properties of the first-order vector semi-rational rogue waves with $\mu(t)$ and $\gamma(t)$ chosen as the constants. Figures 1(a1) and 1(a2) demonstrate that a four-petalled rogue wave exists with an eye-shaped breather. Comparing Figs. 1(b1)–1(b2) or 1(c1)–1(c2) with 1(a1)–1(a2), we observe that the width of the four-petalled rogue wave along the t axis and temporal separation between the adjacent peaks

of the eye-shaped breather both decrease with $\mu(t)$ or $\gamma(t)$.

With $\mu(t)$ and $\gamma(t)$ taken as the linear functions of t, figure 2 displays the first-order vector semi-rational nonautonomous rogue waves which describe the interactions between the eye-shaped breathers and composite rogue waves. Figures 2(a1) and 2(a2) show the interaction between the breather and the rogue wave with one hump and one valley, where the breather becomes bent, and the temporal separation between two adjacent peaks increases around the interaction part. With $\mu(t) = \left(t+\sqrt{3}\right)/2$ and $\gamma(t) = \left(t+\sqrt{3}\right)/50$, figures 2(b1) and 2(b2) illustrate the interaction between the breather and the composite rogue wave with two humps and two valleys, where the two adjacent peaks of the breather merge into one peak at the interaction part. Increasing the intercepts of $\mu(t)$ and $\gamma(t)$, we observe that the double-peak structure appears at the interaction part for the breather, as seen in Figs. 2(c1) and 2(c2).

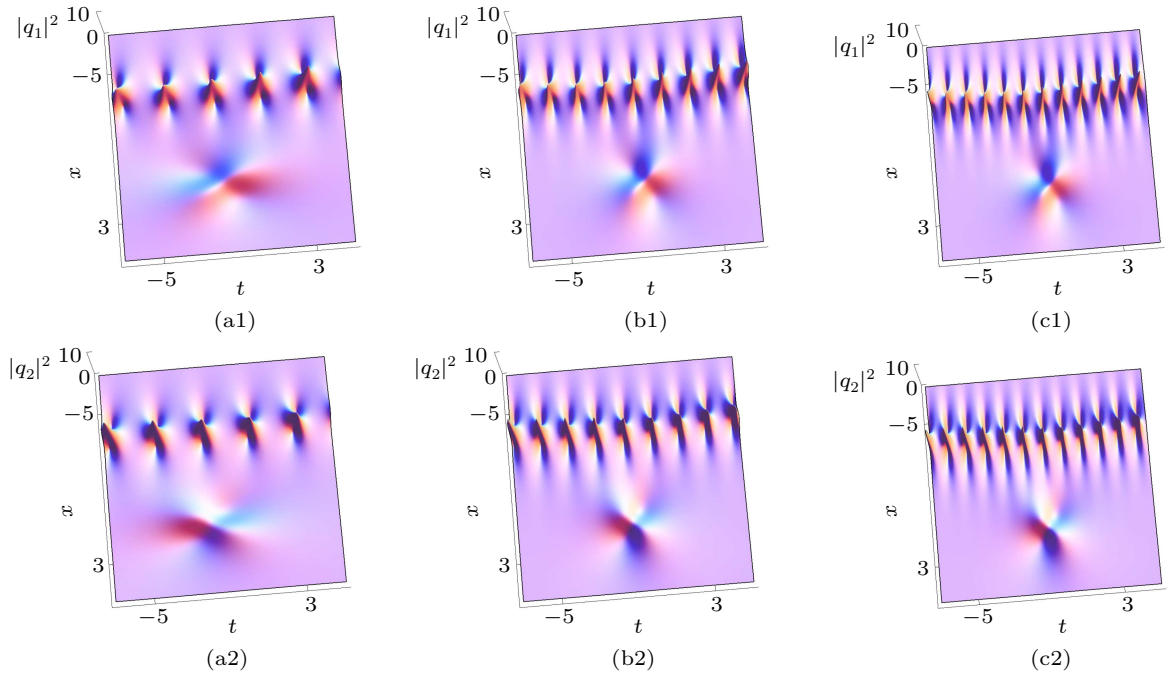

Fig. 1. The first-order vector semi-rational rogue waves via solutions (9) with $N = 1$, $l_{11} = 1$, $l_{21} = 1$, $l_{31} = 1/100$, (a1), (a2) $\mu(t) = 1/2$, $\gamma(t) = 1/50$; (b1), (b2) $\mu(t) = 1$, $\gamma(t) = 1/50$; (c1), (c2) $\mu(t) = 1/2$, $\gamma(t) = 1/10$.

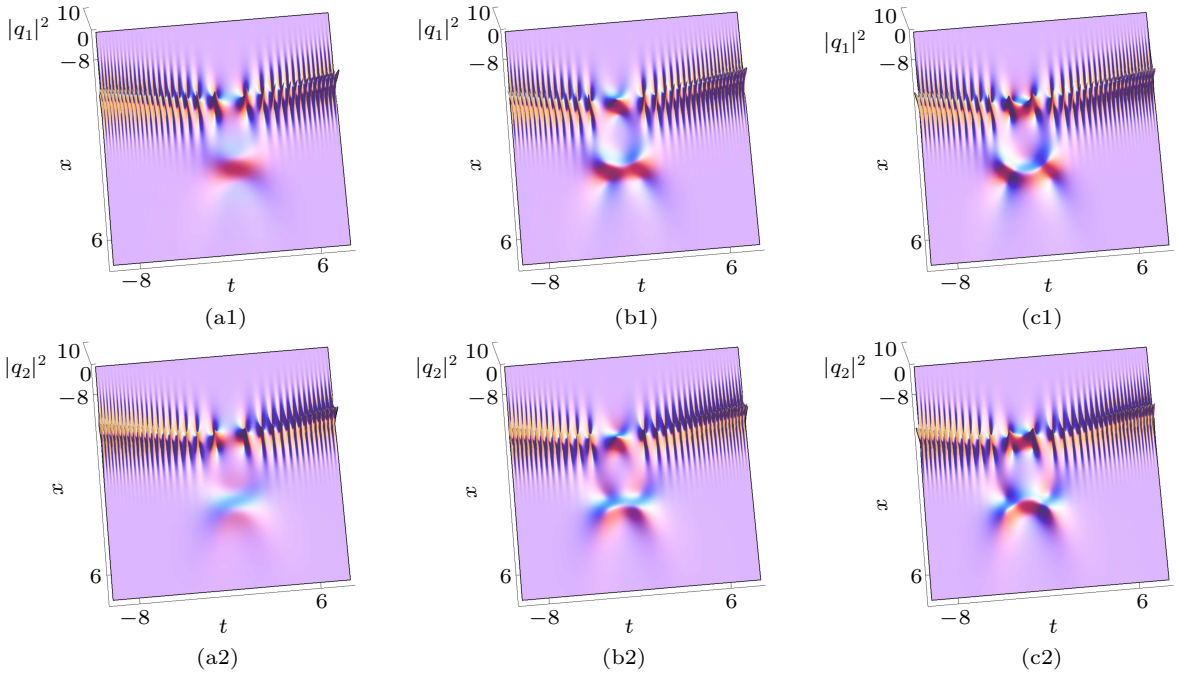

Fig. 2. The first-order vector semi-rational nonautonomous rogue waves via solutions (9) with $N = 1$, $l_{11} = 1$, $l_{21} = 1$, $l_{31} = 1/100$, (a1), (a2) $\mu(t) = t/2$, $\gamma(t) = t/50$; (b1), (b2) $\mu(t) = \frac{1}{2}\left(t+\sqrt{3}\right)$, $\gamma(t) = \frac{1}{50}\left(t+\sqrt{3}\right)$; (c1), (c2) $\mu(t) = \frac{1}{2}\left(t+\frac{6\sqrt{3}}{5}\right)$, $\gamma(t) = \frac{1}{50}\left(t+\frac{6\sqrt{3}}{5}\right)$.

When $\mu(t)$ and $\gamma(t)$ are the cosine functions, the first-order periodic vector semi-rational rogue waves are presented in Figs. 3. Figures 3(a1) and 3(a2) exhibit the existence of the eye-shaped breather and the periodic rogue wave with one hump and one valley in each component. With the periods of $\mu(t)$ and $\gamma(t)$ increasing, the temporal separation between two adjacent peaks of the breather and the period of the periodic rogue wave both increase, as presented in Figs. 3(b1) and 3(b2). When we continue to increase the periods of $\mu(t)$ and $\gamma(t)$, the period of the vector periodic semi-rational nonautonomous rogue wave also keeps increasing, and each intermingled peak of the breather branches out into two separated peaks, as displayed in Figs. 3(c1) and 3(c2).

In Fig. 4, we present the first-order asymmetry vector semi-rational rogue waves when $\mu(t)$ and $\gamma(t)$ are the exponential functions of t. When $\mu(t) = \mathrm{e}^{-t/5}/2$ and $\gamma(t) = \mathrm{e}^{-t/5}/50$, figures 4(a1) and 4(a2) show that an asymmetry breather with changing velocity coexists with an asymmetry rogue wave, where the asymmetry breather and rogue wave both possess a hump along the positive direction of the t axis.

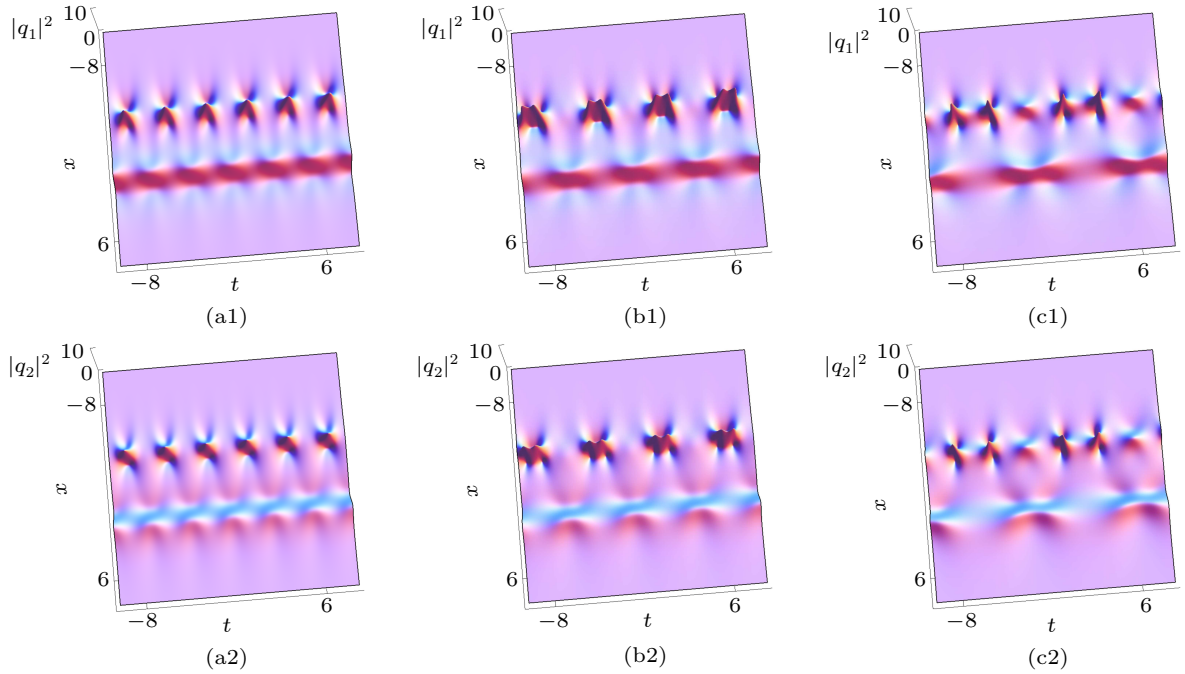

Fig. 3. The same as Fig. 2 except that (a1), (a2) $\mu(t) = \frac{1}{2}\cos 2t$, $\gamma(t) = \frac{1}{50}\cos 2t$; (b1), (b2) $\mu(t) = \frac{1}{2}\cos\frac{5}{4}t$, $\gamma(t) = \frac{1}{50}\cos\frac{5}{4}t$; (c1), (c2) $\mu(t) = \frac{1}{2}\cos\frac{3}{4}t$, $\gamma(t) = \frac{1}{50}\cos\frac{3}{4}t$.

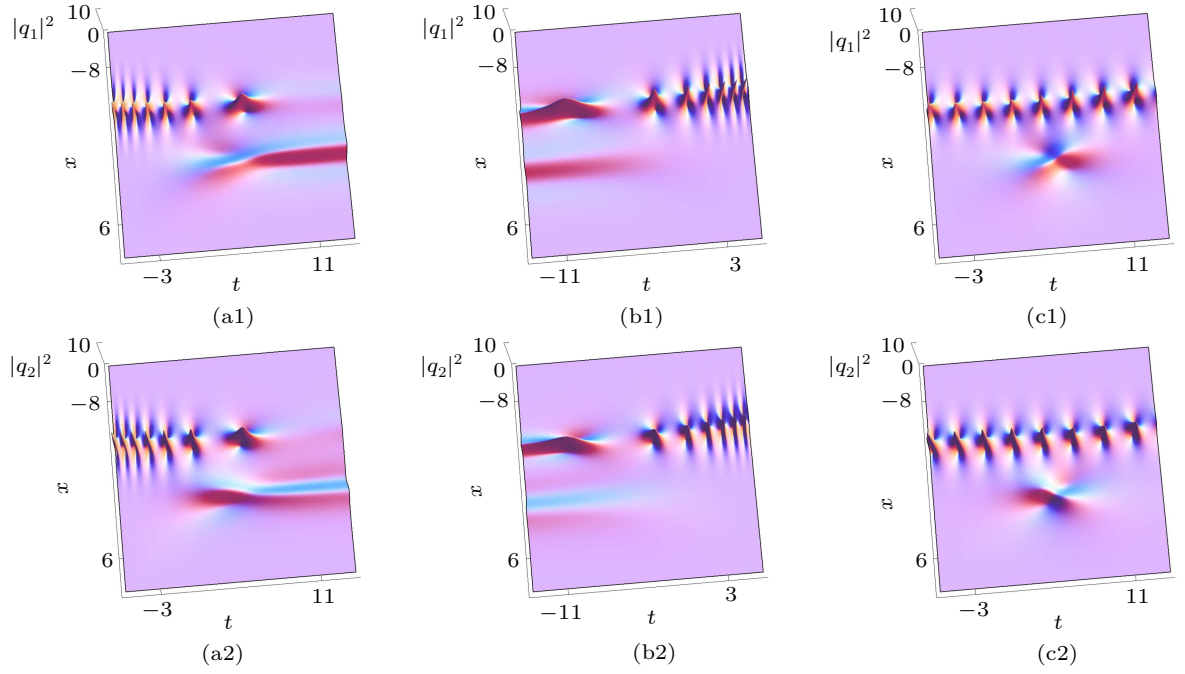

Fig. 4. The same as Fig. 2 except that (a1), (a2) $\mu(t) = \frac{1}{2}\mathrm{e}^{-\frac{t}{5}}$, $\gamma(t) = \frac{1}{50}\mathrm{e}^{-\frac{t}{5}}$; (b1), (b2) $\mu(t) = \frac{1}{2}\mathrm{e}^{\frac{t}{5}}$, $\gamma(t) = \frac{1}{50}\mathrm{e}^{\frac{t}{5}}$; (c1), (c2) $\mu(t) = \frac{1}{2}$, $\gamma(t) = \frac{1}{50}\mathrm{e}^{-\frac{1}{25}(t+\sqrt{3}/3)}$.

When $\mu(t) = e^{t/5}/2$ and $\gamma(t) = e^{t/5}/50$, the asymmetry breather and rogue wave both possess an hump along the negative direction of the t axis, as depicted in Figs. 4(b1) and 4(b2). When $\mu(t) = 1/2$ and $\gamma(t) = e^{-\frac{1}{25}(t+\sqrt{3}/3)}/50$, figures 4(c1) and 4(c2) describe the interaction between the four-petalled rogue wave and asymmetry breather, where the height for the peak of the breather decreases along the positive direction of the t axis.

4.2. The second-order vector semi-rational nonautonomous rogue waves

With $\mu(t)$ and $\gamma(t)$ being the constants, figures 5(a1) and 5(a2) depict the second-order vector semi-rational rogue waves, which demonstrate that the triangle structure composed of three four-petalled rogue waves coexist with two eye-shaped breathers. As $\mu(t)$ or $\gamma(t)$ increases, the width of the triangle structure along the t axis and the temporal separation between the adjacent peaks of each eye-shaped breather both decrease, as presented in Figs. 5(b1), 5(b2), 5(c1), and 5(c2).

Figure 6 shows the second-order vector semi-rational nonautonomous rogue waves with $\mu(t)$ and $\gamma(t)$ being different functions. When $\mu(t)$ and $\gamma(t)$ are the linear functions, figures 6(a1) and 6(a2) exhibit the interaction between the two breathers and the quadrangle structure, which is constituted by two four-petalled rogue waves and two rogue waves with one hump and one valley. When $\mu(t)$ and $\gamma(t)$ are taken as

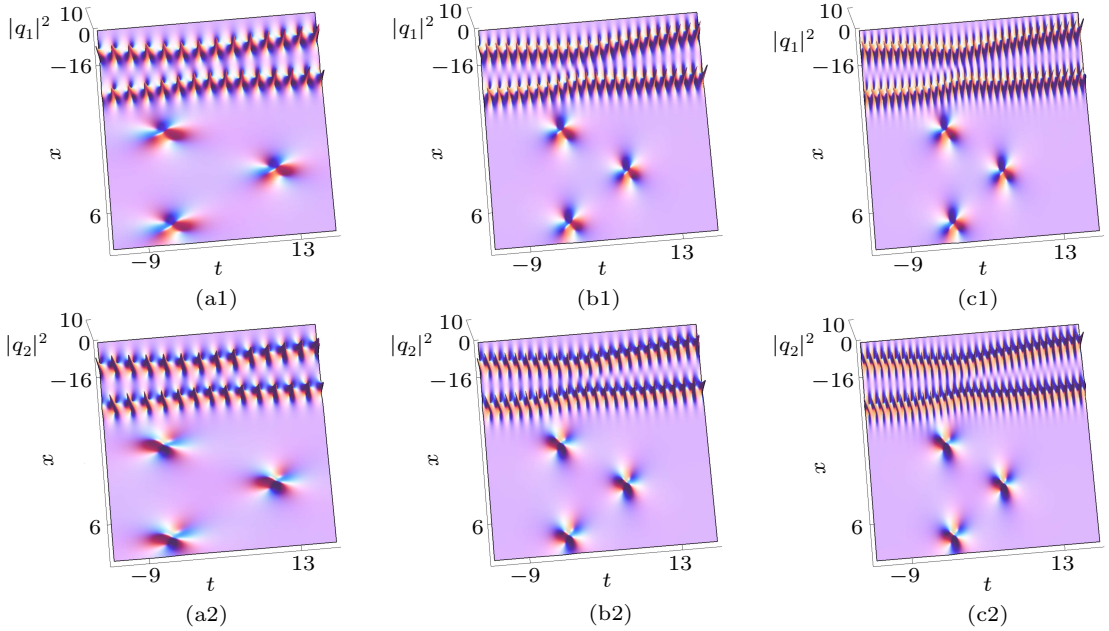

Fig. 5. The second-order vector semi-rational rogue waves via solutions (9) with $N = 2$, $l_{11} = 0$, $l_{12} = 100$, $l_{21} = 1$, $l_{22} = 0$, $l_{31} = 10^{-8}$, $l_{32} = 0$, (a1), (a2) $\mu(t) = 1/2$, $\gamma(t) = 1/50$; (b1), (b2) $\mu(t) = 1$, $\gamma(t) = 1/50$; (c1), (c2) $\mu(t) = 1/2$, $\gamma(t) = 1/10$.

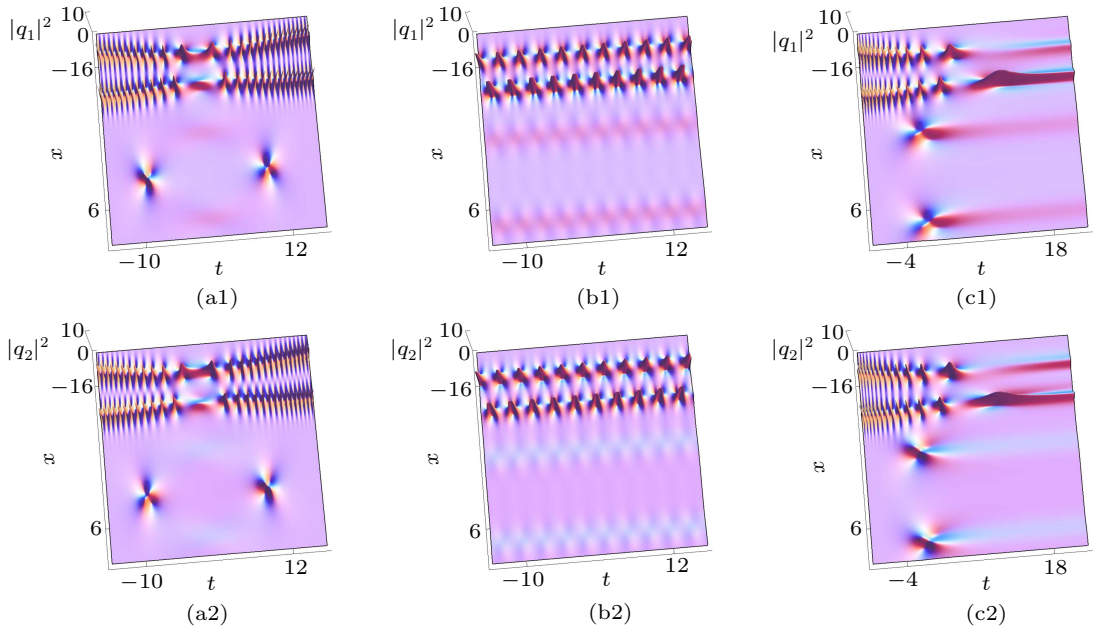

Fig. 6. The same as Fig. 5 except for (a1), (a2) $\mu(t) = \frac{1}{8}t$, $\gamma(t) = \frac{1}{200}t$; (b1), (b2) $\mu(t) = \frac{1}{2}\cos 2t$, $\gamma(t) = \frac{1}{50}\cos 2t$; (c1), (c2) $\mu(t) = \frac{1}{2}e^{-\frac{t}{5}}$, $\gamma(t) = \frac{1}{50}e^{-\frac{t}{5}}$.

the cosine functions, figures 6(b1) and 6(b2) display the second-order periodic semi-rational rogue wave which describes that the two parallel eye-shaped breathers coexist with two parallel periodic rogue waves with one hump and one valley in each component. When $\mu(t)$ and $\gamma(t)$ are chosen as the exponential functions, figure 6(c1) and 6(c2) present the second-order asymmetry vector semi-rational rogue wave which is formed by two asymmetry four-petalled rogue waves and two asymmetry eye-shaped breathers in each component.

5. Conclusions

Optical fibers have been seen in the optical sensing and optical fiber communication. Simultaneous propagation of optical pulses in an inhomogeneous optical fiber has been beleived to be described by a coupled time-dependent coefficient fourth-order nonlinear Schrödinger system, i.e., system (1), which has been discussed in this paper. For system (1), we have worked out Lax pair (2) which is distinct from that in Ref. [30], the N-th-order DT (4), and the N-th-order vector semi-rational nonautonomous rogue wave solutions under coefficient conditions (3), i.e., solutions (9). By dint of solutions (9), we have graphically investigated the first- and second-order vector semi-rational nonautonomous rogue waves with the GVD coefficient $\mu(t)$ and FOD coefficient $\gamma(t)$.

By means of solutions (9) with $N=1$, figure 1 has shown the first-order vector semi-rational rogue waves with $\mu(t)$ and $\gamma(t)$ being the constants: width of the four-petalled rogue wave along the t axis and temporal separation between the adjacent peaks of the eye-shaped breather both decrease with $\mu(t)$ or $\gamma(t)$; with $\mu(t)$ and $\gamma(t)$ chosen as the linear functions, figure 2 has displayed the first-order vector semi-rational nonautonomous rogue waves which describe the interactions between the eye-shaped breathers and the composite rogue waves; figure 3 has presented the first-order periodic vector semi-rational rogue waves with $\mu(t)$ and $\gamma(t)$ taken as the cosine functions. When $\mu(t)$ and $\gamma(t)$ are the exponential functions, figure 4 has depicted the first-order asymmetry vector semi-rational rogue waves.

According to solutions (9) with $N=2$, when $\mu(t)$ and $\gamma(t)$ are the constants, figure 5 has depicted the second-order vector semi-rational rogue waves, which demonstrate that the triangle structure composed of three four-petalled rogue waves coexists with the two eye-shaped breathers: width of the triangle structure along the t axis and temporal separation between the adjacent peaks of each eye-shaped breather both decrease with $\mu(t)$ or $\gamma(t)$. When $\mu(t)$ and $\gamma(t)$ are the linear, cosine, and exponential functions, figure 6 has respectively shown the interaction between two eye-shaped breathers and the quadrangle structure constituted by two four-petalled rogue waves and two rogue waves with one hump and one valley, the second-order periodic vector semi-rational rogue waves, and the second-order asymmetry vector semi-rational rogue waves.

References

[1] Kowal D, Urbanczyk W and Mergo P 2018 *Sensors-Basel* **18** 915
[2] Khaykovich L, Schreck F, Ferrari G, Bourdel T, Cubizolles J, Carr L D, Castin Y and Salomon C 2002 *Science* **296** 1290
[3] Lan Z Z and Su J J 2019 *Nonlinear Dyn.* **96** 2535
[4] Musslimani Z H, Makris K G, El-Ganainy R and Christodoulides D N 2008 *Phys. Rev. Lett.* **100** 030402
[5] Xie X Y and Meng G Q 2019 *Eur. Phys. J. Plus* **134** 359
[6] Messouber A, Triki H, Azzouzi F, Zhou Q, Biswas A, Moshokoa S P and Belic M 2018 *Opt. Commun.* **425** 64
[7] Xie X Y , Yang S K, Ai C H and Kong L C 2020 *Phys. Lett. A* **384** 126119
[8] Akhmediev N, Soto-Crespo J M and Ankiewicz A 2009 *Phys. Rev. A* **80** 043818
[9] Mahnke C and Mitschke F 2012 *Phys. Rev. A* **85** 033808
[10] Akhmediev N, Dudley J M, Solli D R and Turitsyn S K 2013 *J. Opt.* **15** 060201
[11] Wang L, Zhang J H, Wang Z Q, Liu C, Li M, Qi F H and Guo R 2016 *Phys. Rev. E* **93** 012214
[12] Wang X B, Tian S F and Zhang T T 2018 *Proc. Am. Math. Soc.* **146** 3353
[13] Solli D R, Ropers C, Koonath P and Jalali B 2007 *Nature* **450** 1054
[14] Wang X B, Tian S F, Feng L L and Zhang T T 2018 *J. Math. Phys.* **59** 073505
[15] Akhmediev N, Ankiewicz A and Taki M 2009 *Phys. Lett. A* **373** 675
[16] Liu Y K and Li B 2017 *Chin. Phys. Lett.* **34** 10202
[17] Zhao L C, Yang Z Y and Yang W L 2019 *Chin. Phys. B* **28** 010501
[18] Chen S, Soto-Crespo J M, Baronio F, Grelu P and Mihalache D 2016 *Opt. Exp.* **24** 15251
[19] Ankiewicz A, Kedziora D J and Akhmediev N 2011 *Phys. Lett. A* **375** 2782
[20] Lecaplain C, Grelu P, Soto-Crespo J M and Akhmediev N 2012 *Phys. Rev. Lett.* **108** 233901
[21] Wang X B and Han B 2020 *J. Phys. Soc. Jpn.* **89** 014001
[22] Baronio F, Degasperis A, Conforti M and Wabnitz S 2012 *Phys. Rev. Lett.* **109** 044102
[23] Degasperis A and Lombardo S 2013 *Phys. Rev. E* **88** 052914
[24] Wang X B and Han B 2019 *Europhys. Lett.* **126** 15001
[25] Zhang G and Yan Z 2019 *Proc. R. Soc. A* **475** 20180625
[26] Zhang G and Yan Z 2018 *Proc. R. Soc. A* **474** 20170688
[27] Zhang G and Yan Z 2018 *Commun. Nonlinear Sci. Numer. Simulat.* **62** 117
[28] Zhong W P, Belić M and Malomed B A 2015 *Phys. Rev. E* **92** 053201
[29] Liu D Y, Tian B and Xie X Y 2017 *Laser Phys.* **27** 035403
[30] Li M Z, Tian B, Qu Q X, Chai H P, Liu L and Du Z 2017 *Superlattice. Microst.* **112** 20
[31] Du Z, Tian B, Chai H P, Sun Y and Zhao X H 2018 *Chaos Soliton. Fract.* **109** 90
[32] Gao X Y 2019 *Appl. Math. Lett.* **91** 165
[33] Gao X Y, Guo Y J and Shan W R 2020 *Appl. Math. Lett.* **104** 106170
[34] Su J J, Gao Y T, Deng G F and Jia T T 2019 *Phys. Rev. E* **100** 042210
[35] Jia T T, Gao Y T, Deng G F and Hu L 2019 *Nonlinear Dyn.* **98** 269
[36] Deng G F, Gao Y T, Su J J, Ding C C and Jia T T 2020 *Nonlinear Dyn.* **99** 1039
[37] Ablowitz M J, Kaup D J, Newell A C and Segur H 1973 *Phys. Rev. Lett.* **31** 125
[38] Guo B, Ling L and Liu Q 2012 *Phys. Rev. E* **85** 026607